analytical chemistry

ARTICLE

pubs.acs.org/ac

Engineering Nanostructured Porous SiO_2 Surfaces for Bacteria Detection via "Direct Cell Capture"

Naama Massad-Ivanir,[†] Giorgi Shtenberg,[‡] Adi Tzur,[‡] Maksym A. Krepker,[†] and Ester Segal*[,†,§]

[†]Department of Biotechnology and Food Engineering, [‡]The Interdepartmental Program of Biotechnology, and [§]The Russell Berrie Nanotechnology Institute, Technion—Israel Institute of Technology, Haifa 32000, Israel

Supporting Information

ABSTRACT: An optical label-free biosensing platform for bacteria detection (*Escherichia coli* K12 as a model system) based on nanostructured oxidized porous silicon ($PSiO_2$) is introduced. The biosensor is designed to directly capture the target bacteria cells on its surface with no prior sample processing (such as cell lysis). The optical reflectivity spectrum of the $PSiO_2$ nanostructure displays Fabry–Pérot fringes characteristic of thin-film interference, enabling direct, real-time observation of bacteria attachment within minutes. The $PSiO_2$ optical nanostructure is synthesized and used as the optical transducer element. The porous surface is conjugated with specific monoclonal antibodies (immunoglobulin G's) to provide the active component of the biosensor. The immobilization of the antibodies onto the biosensor system is confirmed by attenuated total reflectance Fourier transform infrared spectroscopy, fluorescent labeling experiments, and refractive interferometric Fourier transform spectroscopy. We show that the immobilized antibodies maintain their immunoactivity and specificity when attached to the sensor surface. Exposure of these nanostructures to the target bacteria results in "direct cell capture" onto the biosensor surface. These specific binding events induce predictable changes in the thin-film optical interference spectrum of the biosensor. Our preliminary studies demonstrate the applicability of these biosensors for the detection of low bacterial concentrations. The current detection limit of *E. coli* K12 bacteria is 10^4 cells/mL within several minutes.

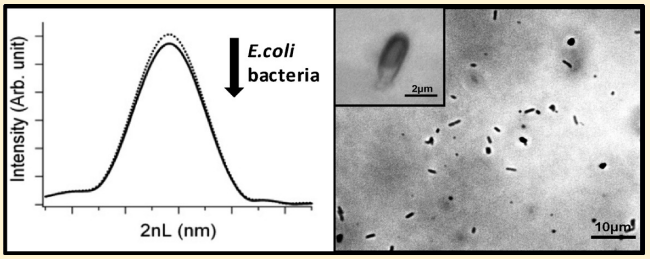

Food- and water-borne bacterial outbreaks remain a major cause for disease and mortality throughout the world.[1,2] Rapid detection of these pathogenic microorganisms is critical for prevention of these outbursts.[3] To date, the detection and identification of pathogens rely mainly on classical culturing techniques or on advanced "rapid" techniques in microbiology, such as biochemical kits, ELISA (enzyme-linked immunosorbent assay), and PCR (polymerase chain reaction) assays.[4,5] These methods are laborious and time-consuming and lack the ability to detect microorganisms in "real time" or outside the laboratory environment.[4,6,7]

Over the past decade, there has been an immense effort to develop new bioassays and biosensors for the rapid detection of food- and water-borne pathogens.[8,9] Various biosensors for rapid identification of bacteria in food and water have been reported, while the most popular are optical biosensors. These biosensors offer a number of advantages, including speed, selectivity, sensitivity, and reproducibility of the measurement.[3,8] To date, the most successful optical-based biosensors are based on surface plasmon resonance (SPR),[10] whereby biomolecular binding events cause a change in the refractive index that is recognized by a shift in the SPR signal. Another significant advantage of these platforms is that no labeling of the target is required. However, the widespread application of these technologies for bacteria detection is limited mainly by the labor, high cost, and complexity of the SPR biosensor system.[10]

In recent years, the biosensor technology of porous silicon (PSi) has received much attention.[11−23] One of the favorable properties of this nanomaterial is its large surface area (up to 500 m^2/cm^3), which enables large amounts and a variety of biomolecular interactions, including enzymes,[24] DNA fragments,[25] and antibodies,[26] occurring over a small working area, facilitating the miniaturization of the biosensor.[16] The resulting activated surface can be used for several biosensing applications, including the detection of DNA,[25] proteins,[15,18,19,22,25] enzyme activity,[24] and bacteria.[5,13,14,27] PSi optical sensors are based on changes of photoluminescence[14,28] or reflectivity[23,29] upon exposure to the target analyte,[30] which replaces the media in the pores. A change in the refractive index of the film is observed as a modulation in the photoluminescence spectrum or as a wavelength shift in the reflectivity spectrum.

Previous studies on porous Si-based optical biosensors (see, e.g., ref 31) have demonstrated only "indirect" bacteria detection via monitoring protein/DNA fragments that are secreted by the bacteria (therefore, prior lysis of the bacteria is required). Our approach is to directly bind the bacteria to the PSi surface. In this case, changes in the amplitude (intensity)

Received: October 30, 2010
Accepted: March 22, 2011
Published: March 22, 2011

of the reflectivity spectrum of the PSi are correlated to specific immobilization of bacteria cells, "direct cell capture" onto the surface via antibody−antigen interactions. In a recent work, we demonstrated this concept for oxidized PSi/hydrogel hybrids. Preliminary studies showed the applicability of these hybrids for the detection of low bacterial concentrations in the range of 10^3-10^5 cells/mL within minutes.[27] In the present work we explore a more straightforward strategy for the preparation of the biosensor surface using neat oxidized PSi ($PSiO_2$) substrates. We demonstrate rapid detection of *Escherichia coli* K-12 bacteria (as a model system) via a direct cell capture approach onto these biosensors. To achieve this goal, $PSiO_2$ films are synthesized and biofunctionalized with a monoclonal antibody (as the capture probe) using well-established coupling chemistry. Changes in the intensity of the reflectivity spectrum of the $PSiO_2$ transducer are monitored upon exposure to *E. coli* bacteria. Correlation between light intensity and specific capture of the bacteria onto $PSiO_2$ allows for rapid detection and quantification of bacterial contaminations.

EXPERIMENTAL SECTION

Materials. Highly doped p-type Si wafers (0.0008 Ω cm resistivity, ⟨100⟩-oriented, B-doped) were purchased from Siltronix Corp. Aqueous HF (48%) and ethanol absolute were supplied by Merck. Bis(*N*-succinimidyl)carbonate (SC), (3-aminopropyl)triethoxysilane (APTES), and diisopropylethylamine (DIEA) were purchased from Sigma-Aldrich Chemicals. The PBS buffer solution at pH 7.4 was prepared by dissolving 50 mM Na_2HPO_4, 17 mM NaH_2PO_4, and 68 mM NaCl in Milli-Q water (18.2 MΩ). Rabbit immunoglobulin G (IgG), fluorescently tagged antirabbit IgG, fluorescently tagged antimouse IgG, and *E. coli* antibody were purchased from Jackson ImmunoResearch Laboratories Inc. *E. coli* (K-12) bacteria were generously supplied by Prof. Sima Yaron (Technion).

Preparation of Porous SiO_2. Si wafers (single side polished on the ⟨100⟩ face and heavily doped, p-type) are electrochemically etched in a 3:1 (v/v) solution of aqueous HF and ethanol for 30 s at a constant current density of 385 mA/cm^2. Si wafers with an exposed area of 1.33 cm^2 are contacted on the back side with a strip of aluminum foil and mounted in a Teflon etching cell; a platinum mesh is used as the counter electrode. After etching, the surface of the wafer is rinsed with ethanol several times and dried under a dry nitrogen gas. The freshly etched PSi samples are thermally oxidized in a tube furnace (Thermolyne) at 800 °C for 1 h in ambient air.

Scanning Electron Microscopy. High-resolution scanning electron microscopy (HRSEM) micrographs of the neat $PSiO_2$ are obtained using a Carl Zeiss Ultra Plus HRSEM instrument at an accelerating voltage of 1 keV.

Gravimetric Determination of Porosity. Porous SiO_2 samples are weighed on a laboratory microbalance to obtain an initial mass (m_1). The oxidized porous layer is then dissolved in an ethanolic HF solution (3:1, v/v, 48% aqueous HF/ethanol). The sample is then weighed again (m_2), and the porosity (P) is calculated using the following equation:[27,32]

$$P = \frac{V_{total} - V_{SiO_2}}{V_{total}} \quad (1)$$

V_{total}, which is the total volume of the $PSiO_2$ layer, is determined by[27,32]

$$V_{total} = St \quad (2)$$

where S is the wafer area exposed to the HF solution during the electrochemical etching and t is the thickness of the $PSiO_2$ layer as determined by cross-sectional SEM measurement. V_{SiO_2}, which is the volume of the SiO_2 fraction in the $PSiO_2$ layer, is calculated from the following equation:[27,32]

$$V_{SiO_2} = \frac{m_1 - m_2}{d} \quad (3)$$

where d is the density of bulk SiO_2, taken as 2.6 g/cm^3.

Measurement of Interferometric Reflectance Spectra. Interferometric reflectance spectra of the samples are collected using an Ocean Optics charge-coupled device (CCD) USB 4000 spectrometer fitted with a microscope objective lens coupled to a bifurcated fiber-optic cable. A tungsten light source is focused onto the center of the sample surface with a spot size of approximately 1−2 mm^2. Reflectivity data are recorded in the wavelength range of 400−1000 nm, with a spectral acquisition time of 100 ms. Both illumination of the surface and detection of the reflected light are performed along an axis coincident with the surface normal. All the optical experiments are conducted in a fixed cell to ensure that the sample reflectivity is measured at the same spot during all the measurements (the measurements are collected in dry surroundings after the surfaces are dried with nitrogen). Spectra are collected using a CCD spectrometer and analyzed by applying fast Fourier transform (FFT).

Determination of Porosity and Film Thickness by the Spectroscopic Liquid Infiltration Method. The porosity and thickness of the $PSiO_2$ layers are determined using the spectroscopic liquid infiltration method (SLIM) as previously described.[27,32] Briefly, the optical thickness (OT) of the sample is determined from the interferometric reflectance spectrum of the porous film in air and while immersed in different liquids, i.e., hexane, ethanol, and acetone, having refractive indices of 1.372, 1.359, and 1.357, respectively. Fitting the optical parameters derived from the reflective interferometric spectra to a Bruggeman effective medium approximation yields a unique solution for both the porosity and the thickness of the sample. Refractive indices for the different solvents and solutions are measured using a Kruss Optronic refractometer. The refractive index of the SiO_2 portion of the film is assumed to be 1.455.

Biofunctionalization of $PSiO_2$ Scaffolds. *Preparation of APTES-Modified surfaces.* A $PSiO_2$ sample is incubated with an aqueous solution of 42 mM APTES and 56 mM DIEA for 30 min. After the solution is removed, the surface is rinsed with purified water and ethanol for 10 min each and dried under a nitrogen stream.

Preparation of NHS-Modified Surfaces. The APTES-modified surface is immersed in a 10 mM SC solution in acetonitrile for 7 min. It should be noted that this concentration was previously found to minimize the formation of bridging SC.[33] After the solution is removed, the surface is washed extensively with acetonitrile three times for 10 min each and dried under a nitrogen stream.

Preparation of IgG-Modified Surfaces. A 1.5 mg/mL antibody solution (amine-terminated chromo pure rabbit IgG, whole molecule) is diluted 1:50 (v/v) with PBS. The NHS-modified surface is incubated in the solution at room temperature for

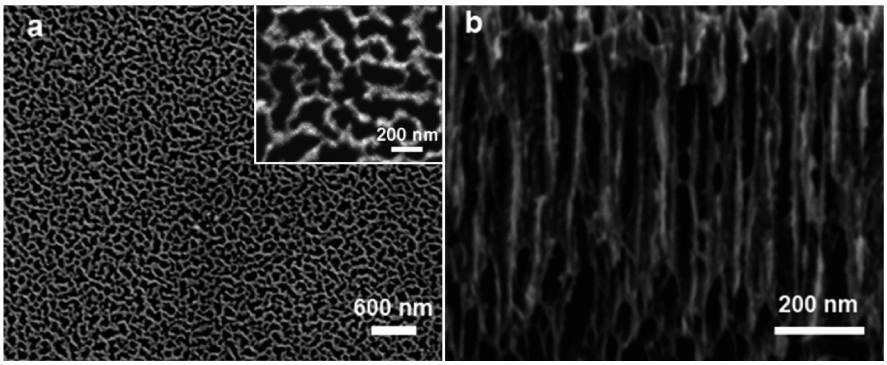

Figure 1. HRSEM micrographs of a typical $PSiO_2$ film etched for 30 s at 385 mA/cm^2: (a) top view, (b) cross-sectional view.

60 min. After the solution is removed, the surface is rinsed with surplus PBS, 1 M NaCl, and PBS for 10 min each.

Infrared Spectroscopy. Surface modification is verified using attenuated total reflectance Fourier transform infrared (ATR-FT-IR) spectroscopy. Spectra are recorded using a Thermo 6700 FT-IR instrument equipped with a Smart iTR diamond ATR device.

Fluorescent Labeling and Fluorescence Microscopy. IgG-modified surfaces are incubated with fluorescently tagged anti-rabbit IgG (1:50, v/v, dilution of the manufacturer's stock solution) for 40 min. IgG-modified surfaces are also incubated with fluorescently tagged antimouse IgG as a control. Following conjugation, the samples are observed under a fluorescence microscope (Nikon TE200-S), and images are taken using a Nikon DMX1200 camera. A constant exposure time of 2 s is used for all measurements. Data are analyzed by the ACT-1 program.

Bacteria Culture. *E. coli* K12 is cultivated in a 10 mL tube with 5 mL of Luria−Bertani (LB) medium (medium composition in 1 L of deionized water: 5 g of NaCl, 5 g of yeast extract, and 10 g of tryptone). The bacteria are incubated overnight at 37 °C with shaking. The bacteria concentration is monitored photometrically by reading the optical density (OD) at a wavelength of 600 nm. After overnight growth in LB medium, the OD_{600} is read using a spectrophotometer to determine the bacterial concentration. The number of cells is directly proportional to the OD_{600} measurements (1 OD_{600} = 10^8 cells/mL). Thus, the bacteria concentration is calculated from the OD_{600} measurements.

Bacteria Sensing. IgG-modified $PSiO_2$ and neat $PSiO_2$ (as the control) samples are incubated with *E. coli* K12 suspensions, ranging from 10^3 to 10^5 cells/mL, for 30 min. These experiments are conducted in a fixed cell to ensure that the sample reflectivity is measured at the same spot during all the measurements. After the bacteria suspension is removed, the cell is flushed for 30 min with a buffer solution. Optical measurements are recorded throughout the experiment. The FFT intensity changes are expressed as percentages and are calculated using the following equation:

$$\text{intensity change } (\%) = \frac{A_1 - A_2}{A_2} \times 100 \qquad (4)$$

where A_1 is the intensity before modification and A_2 is the intensity after modification with the bacteria suspensions.

RESULTS AND DISCUSSION

Preparation and Characterization of $PSiO_2$ Films. The $PSiO_2$ films are prepared from a highly doped p-type crystalline Si wafer, polished on the ⟨100⟩ face using an anodic electrochemical etch, at a constant current density of 385 mA/cm^2 for 30 s. The resulting freshly etched PSi film is then thermally oxidized at 800 °C to create a hydrophilic $PSiO_2$ matrix. The structural properties, i.e., thickness and porosity, of the $PSiO_2$ layer are characterized by three methods, HRSEM, gravimetry (for porosity), and SLIM, as previously described by Massad-Ivanir et al.[27] The average values are summarized in Table S1 (see the Supporting Information). Briefly, the resulting porous layers are 7880 ± 60 nm thick, and the calculated porosity is approximately 80%. HRSEM micrographs of a typical porous layer after thermal oxidation are shown in Figure 1. Top-view micrographs of the $PSiO_2$ film (Figure 1a) reveal its highly porous nature. The cross-sectional SEM micrograph (Figure 1b) of a cleaved film depicts interconnecting cylindrical pores[34,35] ranging in diameter from 60 to 100 nm.

Biofunctionalization of $PSiO_2$ with Monoclonal Antibodies. The synthetic approach for grafting the monoclonal antibodies (IgG) onto the $PSiO_2$ surfaces is based on a well-established silanization technology.[33] The detailed synthesis scheme is outlined in Scheme 1. First, the thermally oxidized surface is aminosilanized by APTES with the aid of an organic base, DIEA, resulting in an aminosilanized surface (Scheme 1a). In the following step, a homobifunctional cross-linker, SC, is incubated with the modified $PSiO_2$ (Scheme 1b). SC reacts with the surface amines of the porous layer through a nucleophilic attack of the amine on C═O succimide ester, eliminating one NHS group. In the final step (Scheme 1c), an amine-terminated rabbit IgG is attached to the surface via the amino-reactive cross-linkers.[33]

To confirm the chemical modification of the SiO_2 scaffold after the different synthetic steps, the samples are characterized using ATR-FT-IR spectroscopy. Figure 2 shows the ATR-FT-IR spectra of the different surfaces (APTES, NHS, IgG). The spectrum of a neat $PSiO_2$ surface (Figure 2, trace a) depicts a typical Si−H vibrating mode at 802 cm^{-1} and a peak at 1056 cm^{-1} that is related to the Si−O−Si stretching mode.[33] The spectrum of the APTES-modified surface (Figure 2, traces b and b(1)) depicts two additional peaks, not observed for the neat $PSiO_2$. The peak at 1641 cm^{-1} is attributed to the bending band of NH_2 and that at 1551 cm^{-1} to the bending band of protonated amines ($-NH_3^+$).[33] These results confirm that APTES is grafted onto the $PSiO_2$ surface. Figure 2, trace c, displays the spectrum of an NHS-modified surface. Amide bands appear at 1631 cm^{-1} (amide I) and 1529 cm^{-1} (amide II), exhibiting a red shift compared to the bending bands of the amines in an APTES-modified surface; refer to Figure 2, trace c(1) vs trace b(1). Two

Scheme 1. Schematic Representation of the Synthesis Steps Followed To Biofunctionalize the $PSiO_2$ Surface with IgG[a]

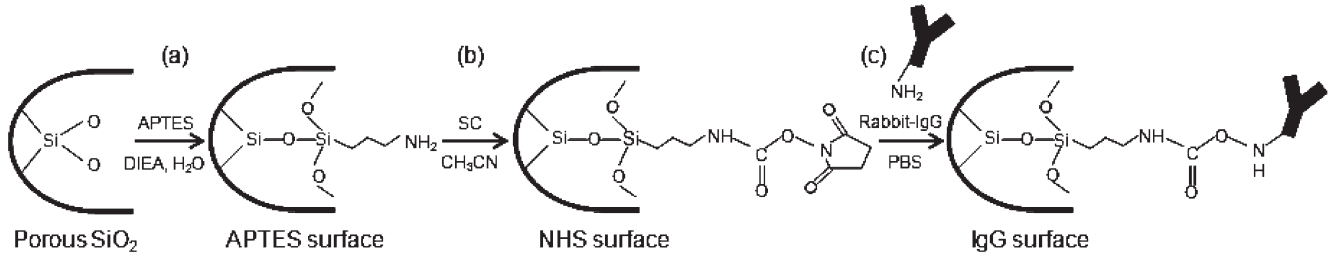

[a] Key: (a) The $PSiO_2$ surface is initially reacted with APTES and is catalyzed by an organic base to create an APTES surface. (b) The APTES surface terminal amine groups react with the NHS activated ester of SC to create an NHS surface. (c) Amine-terminated IgG is attached to the NHS surface to create an IgG surface.

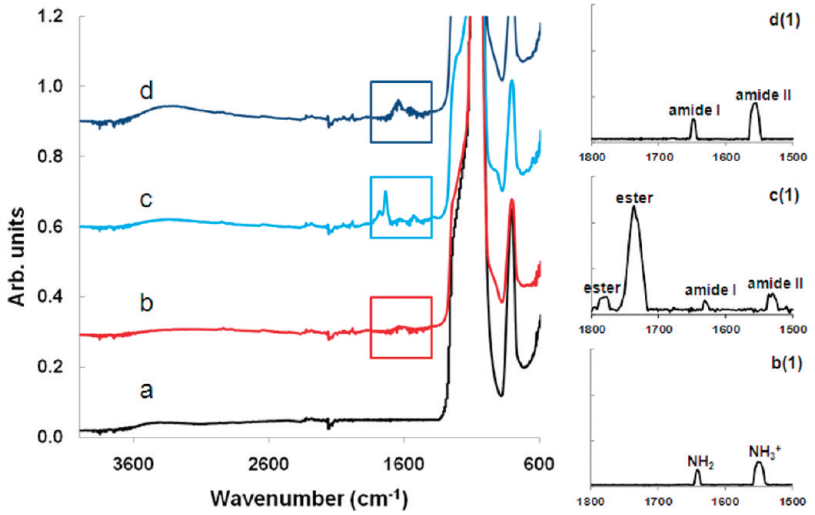

Figure 2. ATR-FT-IR spectra of the (a) neat $PSiO_2$ surface, (b) APTES-modified surface, (c) NHS-modified surface, and (d) IgG-modified surface. Insets b(1), c(1), and d(1) depict the corresponding detailed spectra for clarity (multiplied along the *y* axis).

significant peaks appear at 1737 and 1778 cm^{-1} (Figure 2, trace c(1)), attributed to the asymmetric and symmetric stretching bands of succinimidyl ester, respectively.[33] These results verify that SC is attached to the APTES-modified surface. For the IgG-modified surface (Figure 2, trace d), amide bands appear at 1642 cm^{-1} (amide I) and 1548 cm^{-1} (amide II).[33] These bands show a blue shift compared to the NHS species on the NHS-modified surface, indicating that the IgG molecules are conjugated to the $PSiO_2$ surface.

The attachment of the antibodies to the $PSiO_2$ surface is also confirmed by fluorescent labeling followed by observation of the surface under a fluorescence microscope. Moreover, fluorescence studies also allow us to characterize the activity and antigenic specificity of (rabbit) IgG's conjugated to the $PSiO_2$ surface by binding of fluorescently tagged antirabbit IgG and antimouse IgG as a control. Figure 3 summarizes the results of these experiments. Figure 3a demonstrates that the conjugated rabbit IgG's (as a model for monoclonal antibody) retain their activity after grafting to the surface; the attachment is confirmed by binding of fluorescently tagged antirabbit IgG. In the next set of control experiments (see Figure 3b), the silanization step is omitted and a fluorescent signal is observed, indicating that nonspecific binding of IgG to the surface occurs. Moreover, the nonspecifically immobilized IgG also shows immunogenic activity. This result will be further discussed and confirmed using RIFTS in the following section. When the cross-linker (SC) is omitted from the conjugation scheme (see Figure 3c), no signal is observed, suggesting that the antibodies do not bind to the APTES-modified $PSiO_2$ surface. Additionally, the rabbit IgG-functionalized $PSiO_2$ samples are incubated with a fluorescently tagged antimouse IgG to study the specificity of the surface-immobilized rabbit IgG. No fluorescence is observed, indicating the lack of specificity between the rabbit IgG and the fluorophore (see Figure 3d and Figure S1, Supporting Information).

Reflective Interferometric Fourier Transform Spectroscopy. RIFTS is used as a complementary tool to follow the optical changes occurring during the biofunctionalization of the $PSiO_2$ surface (see Figure 4).[19,27] Briefly, the reflectivity spectrum of the thin PSi layer consists of a series of interference fringes that result from a Fabry–Pérot interference. This fringe pattern arises from reflections at the top and at the bottom of the film, so that the measurement is made over the entire volume of the system. The maxima of these fringes are governed by the following relationship (Fabry–Pérot equation):[20]

$$m\lambda = 2nL \quad (5)$$

The OT refers to the nL term in the Fabry–Pérot formula (where m is an integer, n is the average refractive index, L is the

dx.doi.org/10.1021/ac200407w |*Anal. Chem.* 2011, 83, 3282–3289

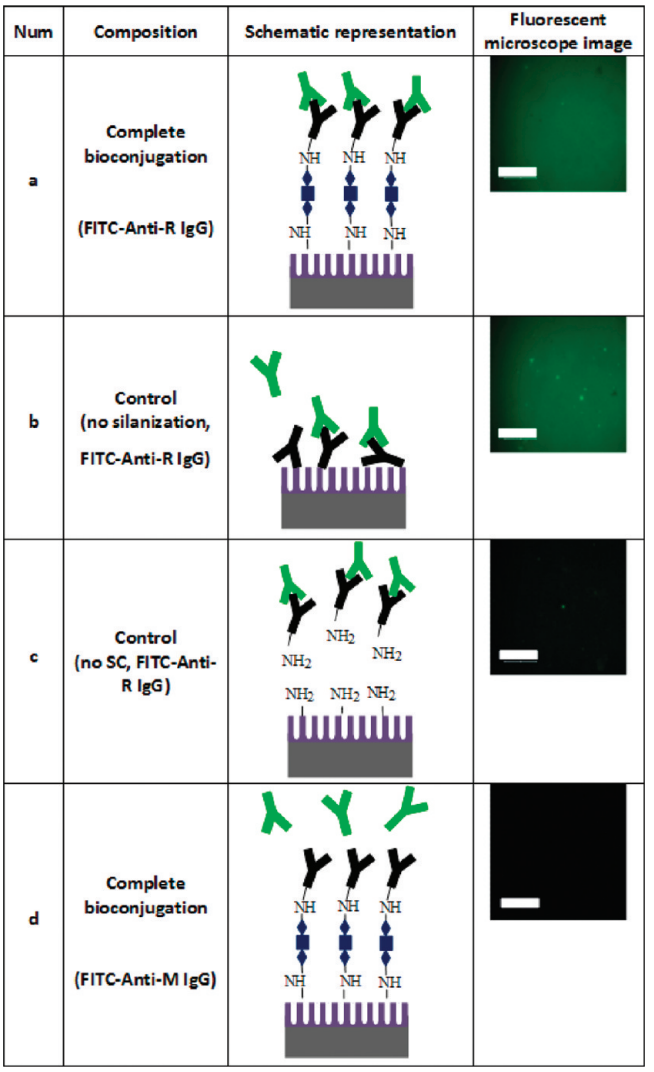

Figure 3. Results of fluorescence labeling experiments to confirm the activity and antigenic specificity of the immobilized IgG. The samples are observed under a fluorescent microscope at a constant exposure time. The scale bar is 100 μm. (a−c) Fluorescence labeling experiments with FITC−antirabbit IgG: (a) complete bioconjugation, $PSiO_2$ + APTES + SC + IgG; (b) control experiment, without silanization, $PSiO_2$ + SC + IgG; (c) control experiment, no cross-linker (SC), $PSiO_2$ + APTES + IgG. (d) Fluorescence labeling experiments with FITC−antimouse IgG: complete bioconjugation, $PSiO_2$ + APTES + SC + IgG. Note: These schematics are for illustration purposes only as conjugation of IgG also occurs inside the pores.

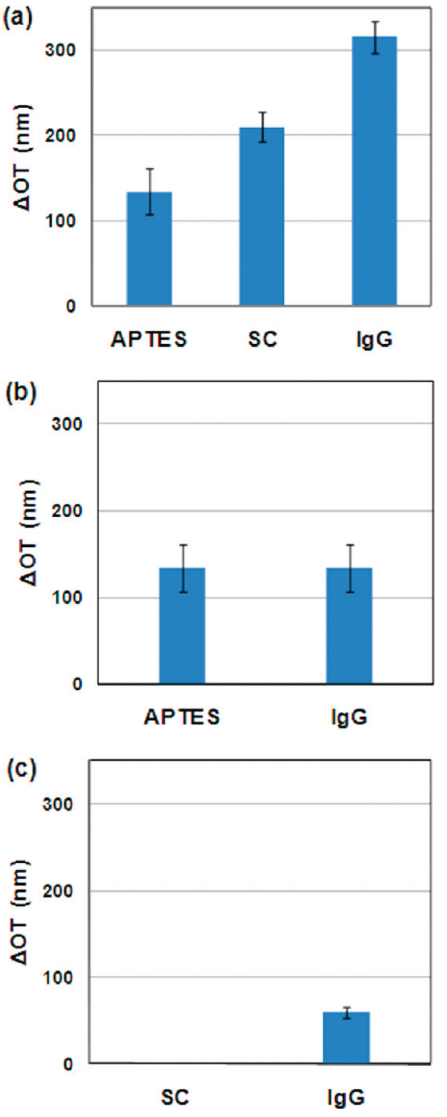

Figure 4. OT changes upon biofunctionalization of $PSiO_2$ with IgG: (a) complete biofunctionalization process; a significant increase in OT is observed after every synthetic step (APTES, SC, IgG) in comparison to that of neat $PSiO_2$; (b) control experiment; no cross-linking agent SC is used; (c) control experiment; no APTES is used (silanization step).

thickness of the film, and λ is the wavelength of the incident light). A change in the average refractive index (n) leads to a shift in the observed reflectivity spectrum that correlates with OT changes.

It is expected that the chemical modification of the porous nanostructure (as previously outlined in Scheme 1) will result in a red shift of the OT, due to the increase in the average refractive index upon attachment of different species to the pore walls. Therefore, the optical properties of the porous nanostructure provide a means for real-time monitoring of changes occurring due to different chemical modifications and biofunctionalizations.[36]

All RIFTS experiments are conducted in a fixed cell to ensure that the sample reflectivity is measured at the same spot during all the measurements. Spectra are collected using a CCD spectrometer and analyzed by applying FFT. Figure 4 depicts the changes in the OT upon the different biofunctionalization steps (refer to the synthesis scheme outlined in Scheme 1). Indeed, it is observed that each modification step results in a significant increase in the OT value, corresponding to an increase in n. These results support our approach that specific attachment to the $PSiO_2$ surface can be observed by monitoring changes in the OT of the film. Thus, in this case, silanization and binding of the cross-linker and IgG's are confirmed. After the silanization step, an increase of 134 ± 27 nm in the OT value is observed (Figure 4a). Attachment of SC causes an additional OT increase of 76 ± 17 nm (Figure 4a). A further increase of 106 ± 18 nm in the OT value is detected upon IgG incubation followed by a buffer wash (Figure 4a).

One of the main problems of refractive index sensitive methods is the discrimination between specific binding of a target analyte to the immobilized capture probe and interfering

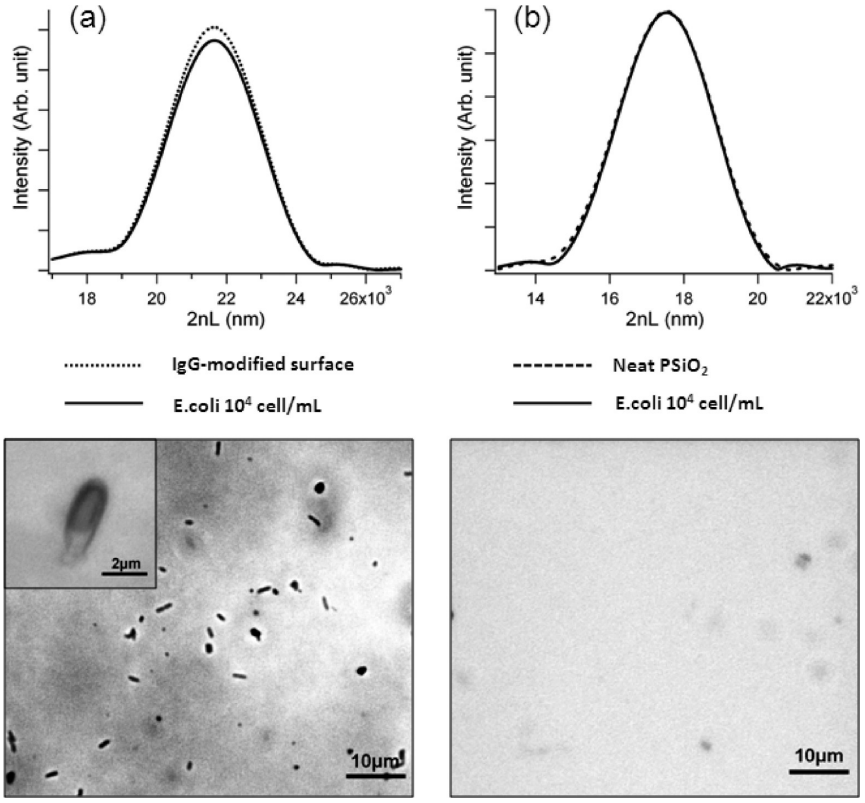

Figure 5. *E. coli* K12 biosensing experiments and corresponding optical microscope images of the biosensors immediately after the experiments. The biosensors are incubated with 10^4 cells/mL *E. coli* suspensions. Key: (a) IgG-modified $PSiO_2$, (b) neat (unmodified) $PSiO_2$.

effects (e.g., nonspecific binding of proteins), which may lead to refractive index changes. Therefore, we have conducted several control experiments to confirm and validate our results. In the first set of control experiments, when no cross-linker (SC) is used, addition of IgG results in insignificant OT changes (Figure 4b). This result indicates that IgG molecules are not immobilized onto the silane-treated $PSiO_2$ film. In the second set of control experiments, no silane coupling agent (APTES) is used. Thus, upon the addition of SC, the OT remains constant (Figure 4c). However, upon the introduction of amine-terminated IgG, a significant red shift of 60 ± 6 nm is observed. This result suggests that the antibodies could adsorb to the surface, supporting the findings of the fluorescence labeling experiments discussed in the previous section (refer to Figure 3b). Moreover, these results are in agreement with previous work on porous SiO_2 surfaces.[18,22,37,38] However, the specific bioconjugation route results in a considerably higher OT increase (more than 100 nm, Figure 4a), suggesting that this IgG immobilization strategy is preferred.

Optical Detection of *E. coli* K-12 Bacteria. Previous sections have demonstrated the construction of a label-free immunosensor based on the immobilization of IgG's onto a $PSiO_2$ nanostructure. We have also confirmed that the immobilized IgG's maintain their immunoactivity and antigenic specificity when attached to the biosensor surface. To show the potential applicability of this platform as a biosensor for the detection of bacteria, we have replaced our model IgG (rabbit IgG) with a specific *E. coli* IgG.

Again, our biosensing approach is based on monitoring changes in the light reflected from the $PSiO_2$ nanostructure. However, in this case, changes in the amplitude (intensity) of the FFT peak of the biosensor are correlated to specific immobilization of bacteria cells, direct cell capture, onto the surface via antibody−antigen interactions.[27] Since *E. coli* bacteria are large biological species, with typical dimensions of $0.8-2\ \mu$m,[39] they are excluded from the pores. Therefore, we expect that binding of bacteria will occur only on the biosensor surface and not inside the porous nanostructure. We have previously demonstrated that specific immobilization of the bacteria cells onto the surface of $PSiO_2$/polyacrylamide hydrogel hybrids results in changes in the light intensity.[27] Herein, we explore two possible strategies for IgG capture probe immobilization onto $PSiO_2$. First, in the nonspecific immobilization route, the *E. coli* IgG's are adsorbed onto a neat $PSiO_2$ surface. In the specific immobilization route, the *E. coli* IgG's are bound onto the $PSiO_2$ surface using the bioconjugation approach discussed in previous sections.

An experimental setup for continuous monitoring of the reflectivity spectrum of the biosensor upon incubation with bacteria suspensions is designed and constructed. The biosensors are exposed to *E. coli* K12 suspensions with different concentrations ranging from 10^3 to 10^5 cells/mL. The incubation time is set to 30 min, after which the samples are washed with a buffer solution for 30 min. Figure 5a (top) displays the FFT spectrum of the biosensor (specific immobilization of *E. coli* IgG) before and after the introduction of the *E. coli* bacteria (10^4 cells/mL). An intensity decrease of $3.4 \pm 0.5\%$ is observed upon exposure to *E. coli*, while insignificant changes in the FFT spectrum are recorded for the unmodified $PSiO_2$ surface (Figure 5b, top). To confirm that this intensity change results from bacteria capture onto the $PSiO_2$ surface, the biosensors are studied under a light microscope immediately after the biosensing experiment. Indeed,

dx.doi.org/10.1021/ac200407w |*Anal. Chem.* 2011, 83, 3282–3289

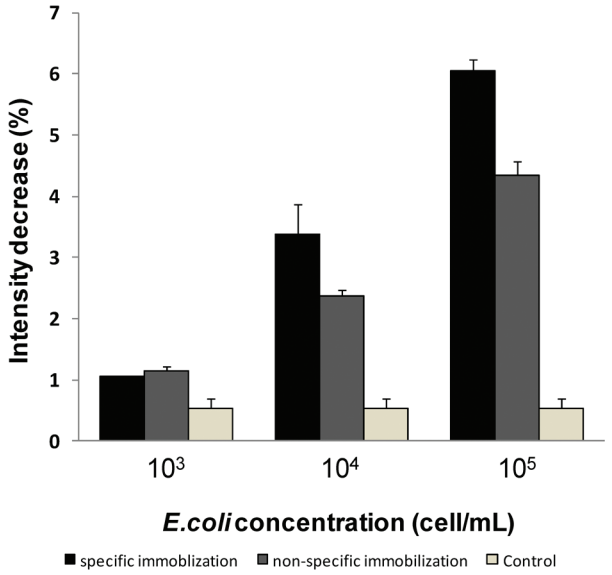

Figure 6. Intensity changes of specific and nonspecific modified $PSiO_2$ upon introduction to different concentrations of *E. coli* K12 bacteria suspensions. The control experiments represent incubation of unmodified $PSiO_2$ with 10^3, 10^4, and 10^5 cells/mL *E. coli* bacteria suspensions.

immobilized bacteria cells are observed on the biosensor surface (see Figure 5a, bottom), while no cells are observed on the unmodified surfaces (control); see Figure 5b, bottom. These results support our approach that direct cell capture of bacteria onto the $PSiO_2$ surface via antibody−antigen interactions can be observed by monitoring changes in the intensity of the reflectivity spectrum.

In Figure 6, the optical response of the biosensors upon the introduction to different concentrations of *E. coli* K12 suspensions is presented. A pronounced effect of the IgG immobilization approach is observed, as the biosensors prepared by specific IgG immobilization exhibit a greater intensity response at all studied concentrations. The intensity signals of all biosensors are proportional to the bacteria suspension concentration. As expected, exposure of the biosensors to a lower bacteria concentration (10^3 cells/mL) results in a signal decrease; i.e., a smaller change in intensity is observed.

It is well established that the immobilization step is crucial in maintaining the conformation and the immunoactivity of the IgG molecules.[40] Many studies have demonstrated that properly oriented antibodies exhibit higher antigen binding capacities in comparison to randomly oriented antibodies.[41] In this study, the nonspecific immobilization route via physical adsorption results in a random attachment of antibodies onto the $PSiO_2$ surface. The random attachment is often associated with antigen binding site modification and denaturation of the antibody.[40−42] On the other hand, in the specific immobilization route the active sites of the antibodies are more stable and better accessible to the target analytes.[43,44] Indeed, the observed performance of the biosensors in terms of their sensitivity toward a specific bacteria loading supports these claims. When comparing the intensity decrease associated with the specific and the nonspecific immobilization strategies (see Figure 6), the specific bioconjugation route results in a significantly higher intensity change after *E. coli* exposure, suggesting that this IgG immobilization strategy is preferred.

In terms of the detection limit of the biosensor, these preliminary experiments show a relatively low detection limit of 10^4 cells/mL. For comparison, the detection limit of current state-of-the-art SPR biosensors is in the range of 10^2 to 10^6 cells/mL.[9,10,45,46] Moreover, the response time of the modified $PSiO_2$ to bacteria exposure is comparable to that of SPR techniques.

We are currently exploring several approaches to enhance the sensitivity of these biosensors, by optimization of antibody concentration and orientation via different coupling chemistries and incorporation of other capture probes, e.g., antimicrobial peptides. Moreover, we are studying several approaches for the introduction of robust secondary assays into these platforms.

CONCLUSIONS

A label-free optical immunosensor, based on a $PSiO_2$ nanostructure (a Fabry−Pérot thin film) is synthesized and characterized, and its potential applicability as a biosensor for bacteria detection is confirmed. A straightforward three-step method for biofunctionalizing the $PSiO_2$ surface with IgG, as a capture probe, is demonstrated. The chemical modification steps and the attachment of the antibodies to the porous surface are confirmed by ATR-FT-IR spectroscopy, fluorescent labeling experiments, and RIFTS. This proof-of-concept work demonstrates that monitoring changes in the thin-film optical interference spectrum of the $PSiO_2$ biosensor enables a simple and sensitive detection scheme of bacteria via a direct cell capture approach. Our preliminary biosensing experiments demonstrate a detection limit of 10^4 cells/mL for *E. coli* and a response time of several minutes. Several approaches are currently being explored to improve the detection limit and sensitivity of the biosensor, including improving optimization of the antibody concentration and orientation, enhancement of the coupling chemistry, and incorporation of a hydrogel into the $PSiO_2$ nanostructure. In conclusion, the work presented here provides a generic biosensing platform that can be translated to many biosensing applications of a variety of microorganisms.

ASSOCIATED CONTENT

Supporting Information. Additional information as noted in the text. This material is available free of charge via the Internet at http://pubs.acs.org.

AUTHOR INFORMATION

Corresponding Author
*E-mail: esegal@tx.technion.ac.il.

ACKNOWLEDGMENT

This work was supported by the Isreal Science Foundation (Grant 1118/08), a Marie Curie Reintegration Grant (NANOPACK) administered by the European Union, and the Wilbush J. Fund. E.S. gratefully acknowledges the generous financial support of the Technion and the Russell Berrie Nanotechnology Institute. We thank Dr. Lisa Bonanno-Young for helpful discussions. The first two authors contributed equally to this work.

REFERENCES

(1) Demuth, A.; Aharonowitz, Y.; Bachmann, T. T.; Blum-Oehler, G.; Buchrieser, C.; Covacci, A.; Dobrindt, U.; Emody, L.; van der Ende, A.; Ewbank, J.; Fernandez, L. A.; Frosch, M.; Garcia-del Portillo, F.; Gilmore, M. S.; Glaser, P.; Goebel, W.; Hasnain, S. E.; Heesemann, J.;

Islam, K.; Korhonen, T.; Maiden, M.; Meyer, T. F.; Montecucco, C.; Oswald, E.; Parkhill, J.; Pucciarelli, M. G.; Ron, E.; Svanborg, C.; Uhlin, B. E.; Wai, S. N.; Wehland, J.; Hacker, J. *Infect., Genet. Evol.* **2008**, *8*, 386–393.

(2) Yousef, A. E. *Principles of Bacterial Detection: Biosensors, Recognition Receptors and Microsystems*; Springer: New York, 2008; pp 31−48.

(3) Velusamy, V.; Arshak, K.; Korostynska, O.; Oliwa, K.; Adley, C. *Biotechnol. Adv.* **2010**, *28*, 232–254.

(4) Doyle, M. P., Beuchat, L. R., Montville, T. J., Eds. *Food Microbiology: Fundamentals and Frontiers*, 2nd ed.; ASM Press: Washington, DC, 2001.

(5) Radke, S. M.; Alocilja, E. C. *IEEE Sens. J.* **2005**, *5*, 744–750.

(6) Glynn, B.; Lahiff, S.; Wernecke, M.; Barry, T.; Smith, T. J.; Maher, M. *Int. J. Dairy Technol.* **2006**, *59*, 126–139.

(7) Leonard, P.; Hearty, S.; Brennan, J.; Dunne, L.; Quinn, J.; Chakraborty, T.; O'Kennedy, R. *Enzyme Microb. Technol.* **2003**, *32*, 3–13.

(8) Lazcka, O.; Del Campo, F. J.; Munoz, F. X. *Biosens. Bioelectron.* **2007**, *22*, 1205–1217.

(9) Skottrup, P. D.; Nicolaisen, M.; Justesen, A. F. *Biosens. Bioelectron.* **2008**, *24*, 339–348.

(10) Taylor, A. D.; Ladd, J.; Homola, J.; Jiang, S. *Principles of Bacterial Detection: Biosensors, Recognition Receptors and Microsystems*; Springer: New York, 2008; pp 83−108.

(11) Jane, A.; Dronov, R.; Hodges, A.; Voelcker, N. H. *Trends Biotechnol* **2009**, *27*, 230–239.

(12) Kilian, K. A.; Boecking, T.; Gooding, J. J. *Chem. Commun.* **2009**, 630–640.

(13) Alvarez, S. D.; Schwartz, M. P.; Migliori, B.; Rang, C. U.; Chao, L.; Sailor, M. J. *Phys. Status Solidi A: Appl. Mater. Sci.* **2007**, *204*, 1439–1443.

(14) Chan, S.; Horner, S. R.; Fauchet, P. M.; Miller, B. L. *J. Am. Chem. Soc.* **2001**, *123*, 11797−11798.

(15) Dancil, K.-P. S.; Greiner, D. P.; Sailor, M. J. *J. Am. Chem. Soc.* **1999**, *121*, 7925–7930.

(16) Janshoff, A.; Dancil, K. P. S.; Steinem, C.; Greiner, D. P.; Lin, V. S. Y.; Gurtner, C.; Motesharei, K.; Sailor, M. J.; Ghadiri, M. R. *J. Am. Chem. Soc.* **1998**, *120*, 12108–12116.

(17) Orosco, M. M.; Pacholski, C.; Miskelly, G. M.; Sailor, M. J. *Adv. Mater.* **2006**, *18*, 1393–1396.

(18) Pacholski, C.; Sartor, M.; Sailor, M. J.; Cunin, F.; Miskelly, G. M. *J. Am. Chem. Soc.* **2005**, *127*, 11636–11645.

(19) Pacholski, C.; Yu, C.; Miskelly, G. M.; Godin, D.; Sailor, M. J. *J. Am. Chem. Soc.* **2006**, *128*, 4250–4252.

(20) Sailor, M. J.; Link, J. R. *Chem. Commun.* **2005**, 1375–1383.

(21) Schwartz, M. P.; Derfus, A. M.; Alvarez, S. D.; Bhatia, S. N.; Sailor, M. J. *Langmuir* **2006**, *22*, 7084–7090.

(22) Schwartz, M. P.; Alvarez, S. D.; Sailor, M. J. *Anal. Chem.* **2007**, *79*, 327–334.

(23) Stewart, M. P.; Buriak, J. M. *Adv. Mater.* **2000**, *12*, 859–869.

(24) DeLouise, L. A.; Kou, P. M.; Miller, B. L. *Anal. Chem.* **2005**, *77*, 3222–3230.

(25) Zhang, D.; Alocilja, E. C. *IEEE Sens. J.* **2008**, *8*, 775–780.

(26) Bonanno, L. M.; DeLouise, L. A. *Langmuir* **2007**, *23*, 5817–5823.

(27) Massad-Ivanir, N.; Shtenberg, G.; Zeidman, T.; Segal, E. *Adv. Funct. Mater.* **2010**, *20*, 2269–2277.

(28) de Leon, S. B.; Sa'ar, A.; Oren, R.; Spira, M. E.; Yitzchaik, S. *Appl. Phys. Lett.* **2004**, *84*, 4361–4363.

(29) Archer, M.; Christophersen, M.; Fauchet, P. M. *Biomed. Microdevices* **2004**, *6*, 203–211.

(30) D'Auria, S.; de Champdore, M.; Aurilia, V.; Parracino, A.; Staiano, M.; Vitale, A.; Rossi, M.; Rea, I.; Rotiroti, L.; Rossi, A. M.; Borini, S.; Rendina, I.; De Stefano, L. *J. Phys.: Condens. Matter* **2006**, *18*, S2019–S2028.

(31) Ouyang, H.; DeLouise, L. A.; Miller, B. L.; Fauchet, P. M. *Anal. Chem.* **2007**, *79*, 1502–1506.

(32) Segal, E.; Perelman, L. A.; Cunin, F.; Di Renzo, F.; Devoisselle, J. M.; Li, Y. Y.; Sailor, M. J. *Adv. Funct. Mater.* **2007**, *17*, 1153–1162.

(33) Xia, B.; Xiao, S. J.; Guo, D. J.; Wang, J.; Chao, M.; Liu, H. B.; Pei, J.; Chen, Y. Q.; Tang, Y. C.; Liu, J. N. *J. Mater. Chem.* **2006**, *16*, 570–578.

(34) Bisi, O.; Ossicini, S.; Pavesi, L. *Surf. Sci. Rep.* **2000**, *38*, 1–126.

(35) Zhang, X. G. *J. Electrochem. Soc.* **2004**, *151*, C69–C80.

(36) Anglin, E. J.; Cheng, L. Y.; Freeman, W. R.; Sailor, M. J. *Adv. Drug Delivery Rev.* **2008**, *60*, 1266–1277.

(37) Zangooie, S.; Bjorklund, R.; Arwin, H. *Thin Solid Films* **1998**, *313*, 825–830.

(38) Arwin, H.; Gavutis, M.; Gustafsson, J.; Schultzberg, M.; Zangooie, S.; Tengvall, P. *Phys. Status Solidi A: Appl. Res.* **2000**, *182*, 515–520.

(39) Sundararaj, S.; Guo, A.; Habibi-Nazhad, B.; Rouani, M.; Stothard, P.; Ellison, M.; Wishart, D. S. *Nucleic Acids Res.* **2004**, *32*, D293–D295.

(40) Somasundaran, P. *Encyclopedia of Surface and Colloid Science*, 2nd ed.; CRC Press: Bocal Raton, FL, 2006.

(41) Jung, Y.; Jeong, J. Y.; Chung, B. H. *Analyst* **2008**, *133*, 697–701.

(42) Cha, T.; Guo, A.; Zhu, X. Y. *Proteomics* **2005**, *5*, 416–419.

(43) Vijayendran, R. A.; Leckband, D. E. *Anal. Chem.* **2001**, *73*, 471–480.

(44) Wilchek, M.; Miron, T. *J. Biochem. Biophys. Methods* **2003**, *55*, 67–70.

(45) Dudak, F. C.; Boyaci, I. H. *Food Res. Int.* **2007**, *40*, 803–807.

(46) Dudak, F. C.; Boyaci, I. H. *Biotechnol. J.* **2009**, *4*, 1003–1011.